Metal−Semiconductor Hybrid Aerogels: Evolution of Optoelectronic Properties in a Low Dimensional CdSe/Ag Nanoparticle Assembly

5 AUTHORS, INCLUDING:

Lamia Nahar
Virginia Commonwealth University
4 PUBLICATIONS   **2** CITATIONS

SEE PROFILE

Shopan Hafiz
Virginia Commonwealth University
14 PUBLICATIONS   **41** CITATIONS

SEE PROFILE

Indika Arachchige
Virginia Commonwealth University
**30** PUBLICATIONS   **774** CITATIONS

SEE PROFILE

Metal−Semiconductor Hybrid Aerogels: Evolution of Optoelectronic Properties in a Low-Dimensional CdSe/Ag Nanoparticle Assembly

Lamia Nahar,[†] Richard J Alan Esteves,[†] Shopan Hafiz,[‡] Ümit Özgür,[‡] and Indika U. Arachchige[*,†]

[†]Department of Chemistry, Virginia Commonwealth University, Richmond, Virginia 23284-2006, United States and [‡]Department of Electrical and Computer Engineering, Virginia Commonwealth University, Richmond, Virginia 23284-3072, United States

ABSTRACT Hybrid nanomaterials composed of metal−semiconductor components exhibit unique properties in comparison to their individual counterparts, making them of great interest for optoelectronic applications. Theoretical and experimental studies suggest that interfacial interactions of individual components are of paramount importance to produce hybrid electronic states. The direct cross-linking of nanoparticles (NPs) via controlled removal of the surfactant ligands provides a route to tune interfacial interactions in a manner that has not been thoroughly investigated. Herein, we report the synthesis of CdSe/Ag heteronanostructures (aerogels) via oxidation induced self-assembly of thiol-coated NPs and the evolution of optical properties as a

function of composition. Three hybrid systems were investigated, where the first and second excitonic energies of CdSe were matched with plasmonic energy of Au or Ag NPs and Ag hollow NPs. Physical characterization of the aerogels suggests the presence of an interconnected network of hexagonal CdSe and cubic Ag NPs. The optical properties of hybrids were systematically examined through UV−vis, photoluminescence (PL), and time-resolved (TR) PL spectroscopic studies that indicate the generation of alternate radiative decay pathways. A new emission (640 nm) from CdSe/Ag aerogels emerged at Ag loading as low as 0.27%, whereas absorption band tailing and PL quenching effects were observed at higher Ag and Au loading, respectively. The TRPL decay time of the new emission (∼600 ns) is markedly different from those of the band-edge (1.83 ± 0.03 ns) and trap-state (1190 ± 120 ns) emission maxima of phase pure CdSe, supporting the existence of alternate radiative relaxation pathways in sol−gel derived CdSe/Ag hybrids.
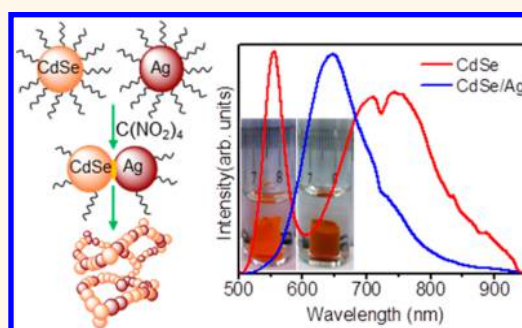
KEYWORDS: sol−gel synthesis · metal−semiconductor hybrids · bandgap · photoluminescence · nanoparticle assembly

Control over the optical properties of semiconductors has been an ever increasing demand to the scientific community. This ongoing thrust has led to the synthesis of nanoscale semiconductors that exhibit size, shape, and composition-dependent photophysical properties.[1] However, for many semiconductor systems, more sophisticated control mechanisms are desired to further improve the material properties for optimization in specific studies. As a result, diverse approaches have been utilized to improve the light-matter interactions, including doping with metals[2] and nonmetals,[3−5] alloying with metal and semiconductors,[6,7] and coupling semiconductor and plasmonic nanoparticles (NPs) to produce hybrid nanomaterials (HNMs).[8−12] HNMs are heteronanostructures consisting of two or more chemically different constituents, such as semiconductor−metal, semiconductor−insulator, or semiconductor−semiconductor composites.[13,14] Each component of the hybrid exhibits unique physical properties, which when assembled together demonstrates different characteristics.[15] The integration of plasmonic metals with semiconductors has attracted much attention due to the potential of coupling high-absorption cross-section and size-tunable optical properties of semiconductor NPs with the localized surface plasmon resonance (LSPR) of metal NPs.[14] The coexistence of similar electronic energy levels in metal and semiconductor NPs has been shown to alter the light-matter interactions with the potential to exhibit novel and tunable photophysical properties.[15−17] Hybrid interactions of

metal/semiconductor systems are typically a result of long-range Columbic interactions, dubbed as Förster resonance energy transfer (FRET),[18,19] and are less likely to occur through a direct electron-tunneling effect. The FRET-type interactions have been shown to produce novel absorption properties.[17] However, in many cases, photoluminescence (PL) quenching is observed as the predominant effect.[20–22] As such, metal–semiconductor hybrids with direct contact for electron tunneling have gained noteworthy interest in the search for better control over optoelectronic properties as well as the fundamental understanding of interfacial interactions among chemically different systems.[16]

Semiconductor colloids, as synthesized, contain an organic coating which serves to provide stability in solution and offers the chemical functionality of demand. However, these organic ligands act as insulating layers that prevent the interparticle interactions needed for charge transfer.[17] To observe electronic energy overlap direct interfacial interactions are desired. To date, direct contact between semiconductor and metal components has been studied via production of core/shell nanostructures,[16,17,20] which exhibit PL quenching. On the other hand, the metal-modified semiconductor hybrids are reported to exhibit both PL quenching and enhancement when decorated with Au and Ag NPs, respectively.[20,21] Aerogels derived from Au-modified CdS NPs are reported to exhibit progressive red shifting and PL quenching effects with increasing Au content.[20,21] However, the reported PL spectra exhibit no distinct band-edge features and are more consistent with trap-state emission.[20,21] Conversely, with Ag-modified CdS aerogels an enhancement of PL intensity has been reported, but the emission also appeared to originate from surface traps.[20,21] Further, direct contact of CdTe and Au colloids has also been achieved through photo-oxidation of surfactant ligands where concentration-dependent PL quenching was reported.[22] The PL quenching mentioned above was attributed to nonradiative relaxation of photogenerated exciton; however, FRET has also been proposed as a possible pathway for depletion of emission.[22,23] In previous studies, the ratio of metal to semiconductor was relatively high, and no spatial separation among individual components was maintained. To minimize the FRET effects, it is important to reduce the plasmonic metal concentration and increase the spatial separation.[24] It has become clear that more comprehensive studies in the low loading ranges are needed to observe changes in optical properties without the interference of FRET quenching. A low-dimensional network consisting of metal and semiconductor NPs is anticipated to provide the optimal interactions leading to hybrid energy states and potentially novel optical properties.

Recently, the synthesis of chalcogenide aerogels via oxidation-induced self-assembly of thiol-coated

semiconductor NPs has been reported.[25–27] More recently, our group has extended this strategy for the synthesis of transparent and opaque metal aerogels composed solely of Ag NPs.[28] The gel morphology consists of an open fractal structure with low-dimensional connectivity between the primary nano-sized constituents.[29–31] The interactions between NPs in the aerogels are expected to be intermediate of those of the core/shell and ligand stabilized NP composites with the potential for optimum overlap of electronic states. Herein, we examine the oxidative assembly of CdSe and Ag or Au NPs into aerogel superstructures and monitor changes in optics as a function of composition. A new hybrid emission maxima was detected at 630–640 nm with 0.27% Ag incorporation and minimal changes to absorption properties, whereas progressive red shifts and tailing effects in absorption onsets were noted at higher Ag loading (0.53–1.83%). Time-resolved PL (TRPL) decay time of the hybrid emission ($\sim$600 ns) is significantly different from those of the band-edge (1.83 $\pm$ 0.03 ns) and trap-state (1190 $\pm$ 120 ns) emission maxima of CdSe aerogels, suggesting the generation of an alternate radiative decay pathway.

RESULTS AND DISCUSSION

We have successfully developed a methodology for the synthesis of CdSe/Ag aerogels via oxidation-induced self-assembly of thiolate-coated NP precursors. Luminescent CdSe NPs demonstrating the first and second excitonic transitions at 525–540 and 380–410 nm, respectively (Figure 1), were prepared via a literature method.[32] These NPs were passivated with thiolate (mercaptoundecanoic acid, MUA) ligands under ambient conditions and dispersed in Milli-Q filtered water to produce concentrated (0.04 M CdSe) colloidal sols. The reaction of AgNO$_3$ with NaOH in the presence of L-glutathione (GSH) was utilized to produce Ag$_2$O precursor seeds, which then undergo slow chemical
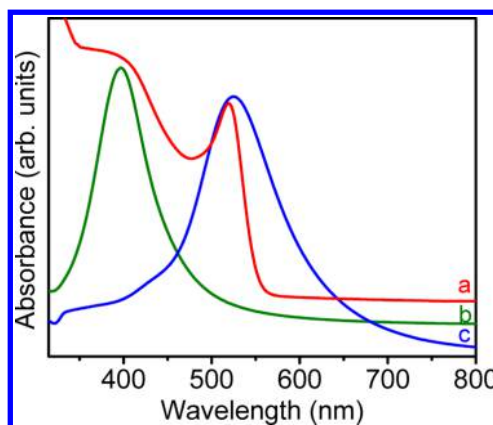

Figure 1. Normalized UV–vis absorption spectra of (a) CdSe and (b) Ag NPs along with (c) hollow Ag NPs demonstrating the overlap of plasmonic resonance of metal NPs with first and second excitonic absorption of CdSe NPs.
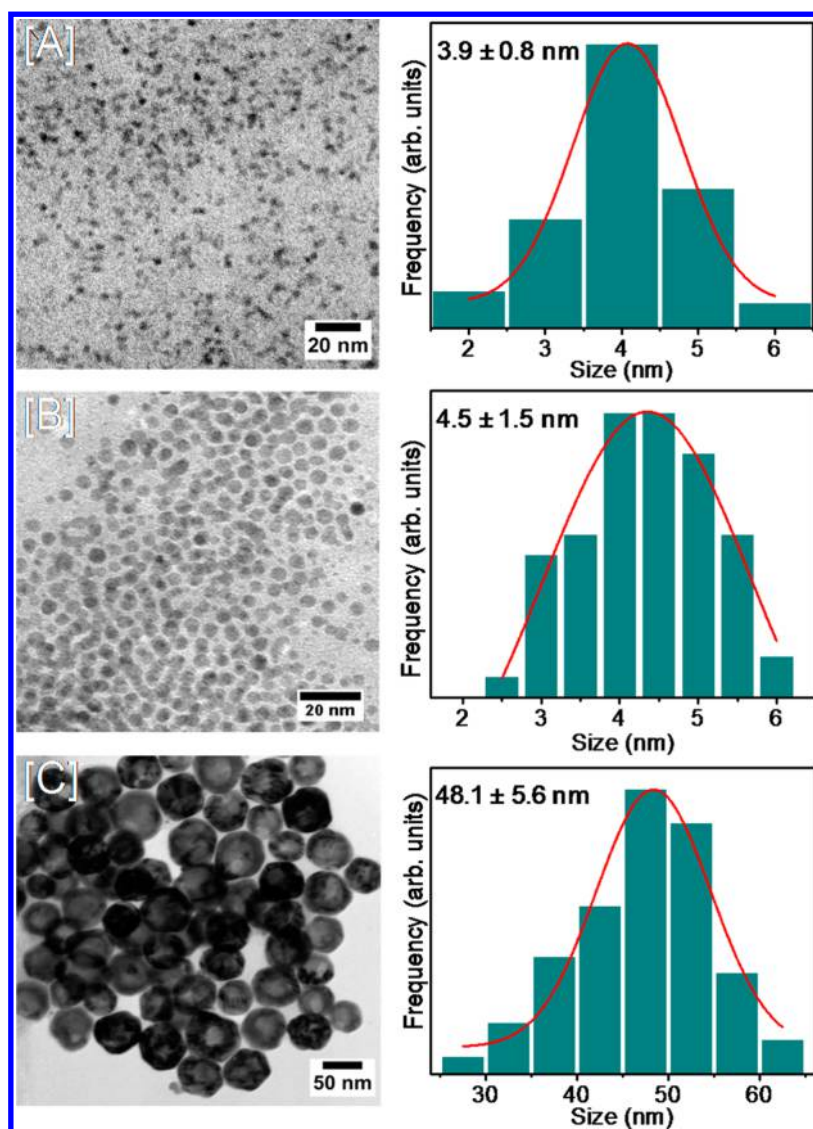
Figure 2. TEM images of the (A) CdSe and (B) Ag NPs along with (C) Ag hollow NPs. The size histograms of respective samples without any postsynthetic size selection are also shown.

reduction to produce solid Ag NPs. Conversely, fast addition of NaBH$_4$ resulted in larger Ag hollows via a Kirkendall-type reaction.[33] For co-gelation, Ag NPs with an average diameter of 4.5 ± 1.5 nm and surface plasmon resonance (SPR) near 390−410 nm were produced to have comparable size with CdSe NPs (3.9 ± 0.8 nm, Figure 2A,B) and spectral overlap of plasmonic and second excitonic energies (Figure 1). In contrast, Ag hollow NPs[28] with 48.0 ± 5.6 nm outer diameter and 10.4 ± 1.4 nm (Figure 2C) shell thickness were prepared to match the spectral overlap of Ag SPR with the first excitonic energy (Figure 1). The capping ligands on NP surface (CdSe with MUA and Ag with GSH) have been chosen to ensure high stability of colloids in water (0.04 M CdSe and 0.004 M Ag) and to enable efficient decomplexation when treated with a non-oxygen transfer oxidant (C(NO$_2$)$_4$).[32] It has been reported that C(NO$_2$)$_4$ oxidizes the thiolates to sulfenyl nitrate as an intermediate (eqs 1 and 2), which then

undergoes reaction with another thiol moiety to produce disulfides,[34] creating active sites on the NP surface (Scheme 1). The formed active sites are highly reactive, allowing the NPs to physically connect to each other yielding CdSe/Ag hydrogels (Figure 3). As prepared hydrogels were supercritically dried to produce CdSe/Ag aerogels (Supporting Information, Figure S1).[26,28] The monolithic aerogels were orange to reddish brown in color and exhibit densities ($d_{\text{CdSe}} - d_{\text{CdSe/Ag}}$) as low as 0.032−0.072 g/cm^3, representing ∼0.55−1.16% of the density of corresponding CdSe/Ag bulk composites. Interestingly, with increasing Ag content the density of CdSe/Ag aerogels has progressively increased owing to slower gelation rate observed with increasing Ag NP incorporation. This can be attributed to differences in oxidation kinetics of surface thiolates (CdSe−MUA vs Ag−GSH) and subsequent changes in NP aggregation that can potentially delay the co-gelation. The longer time required to

Scheme 1. Schematic Representation of the Synthesis of CdSe/Ag Aerogels[a]
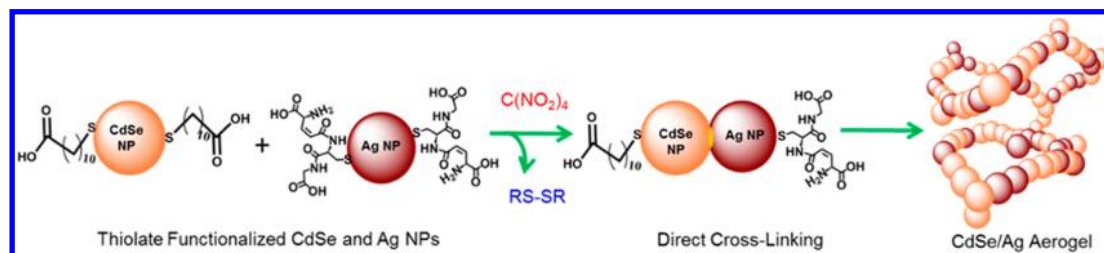
[a] The active sites generated upon oxidative removal of surface thiolates will directly cross-link to produce fractal NP networks and consequently a CdSe/Ag hybrid aerogel. RS−SR = disulfide.
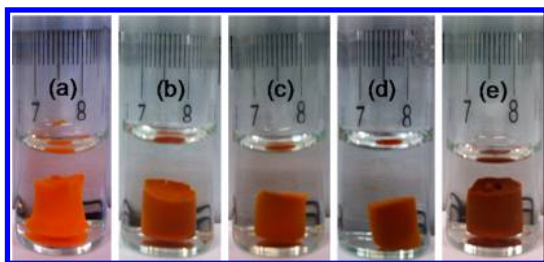

Figure 3. Photographs of CdSe/Ag hydrogels with varying Ag content: (a) 0, (b) 0.33, (c) 0.65, (d) 1.59, and (e) 2.01%. The elemental compositions were obtained from inductively coupled plasma−optical emission spectroscopy (ICP−OES) analysis of corresponding CdSe/Ag aerogels. The scale bar is in centimeters.

Figure 4. PXRD patterns of (A) CdSe/Ag aerogel (2.21% Ag by ICP−OES) along with precursor (B) Ag NPs and (C) CdSe NPs. The ICDD−PDF overlays of hexagonal CdSe (black, PDF no. 08-0459) and cubic Ag (gray, PDF no. 01-0870-719) are shown as vertical lines.

produce CdSe/Ag hydrogels leads to compaction and syneresis (solvent expulsion)[29] resulting in a systematic increase in density of corresponding CdSe/Ag hybrids.

$$RSH + C(NO_2)_4 \rightarrow RS(NO)_2 + C(NO_2)_3{}^- + H^+ \qquad (1)$$

$$RSH + RS(NO)_2 \rightarrow RS-SR + NO_2{}^- + H^+ \qquad (2)$$
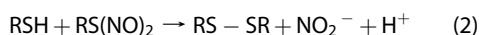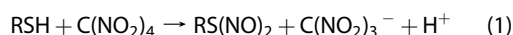
To probe the structure and crystallinity of hybrid aerogels powder X-ray diffraction (PXRD) was employed. Diffraction patterns of CdSe/Ag hybrids indicate the presence of hexagonal CdSe and cubic Ag, consistent with the crystal structures of NP precursors. At low Ag concentrations (0.53−1.83%, ICP−OES analysis), the Bragg reflections corresponding to Ag were not observed, whereas with increasing Ag content, typically >2%, characteristic cubic Ag reflections were observed along with hexagonal CdSe (Figure 4A). Crystallite sizes of the metal and semiconductor components in the hybrids were estimated by applying the Scherrer formula[35] to (110) and (111) reflections of CdSe and Ag, respectively. A slight decrease in crystallite size of both components was noted upon co-gelation and supercritical drying, which has been previously attributed to oxidative etching of CdSe NPs[26,36] and dissolution of Ag by in situ generated HNO$_3$,[28] respectively. The absence of Bragg reflections corresponding to metal oxides or any other elemental impurities suggests that the co-gelation has no impact on the structure and crystallinity of precursor colloids (Figure 4).
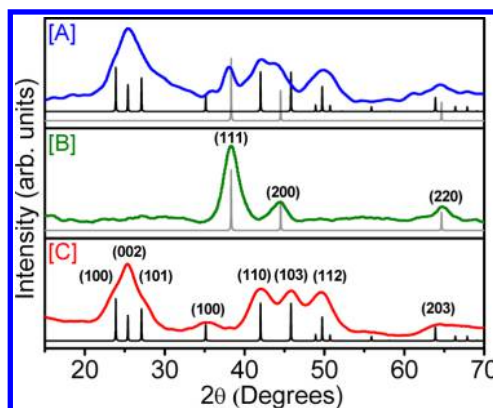
The binding energies of elemental components obtained from X-ray photoelectron spectroscopy (XPS) are in close agreement with those of CdSe[36] and Ag[28] aerogels reported elsewhere. At 1.83% Ag (ICP−OES analysis) loading, the CdSe/Ag hybrids exhibit binding energies of 405.1 eV (Cd 3d$_{5/2}$) and 411.9 eV (Cd 3d$_{3/2}$) and 54.2 eV (Se 3d$_{5/2}$ and 3d$_{3/2}$) (Figure 5), consistent with the phase pure CdSe aerogels produced by the reported method and previous studies on CdSe NPs and aerogel materials.[36] The binding energy of Se 3d (54.2 eV) suggests the presence of reduced Se$_n{}^{n-}$ surface states that have been reported to link CdSe NPs.[36] While there is a distinct absence of CdO$_x$ peaks (3d$_{5/2}$ 403.2 eV),[37,38] in a few samples SeO$_2$ 59.0 eV (Se 3d$_{5/2}$) is present as a result of the oxidative gelation process. Examination of pure Ag NP aerogels specifies the presence of only metallic Ag with binding energies of 367.9 eV (Ag 3d$_{5/2}$) and 373.9 eV (Ag 3d$_{3/2}$) similar to a prior report.[28] Monitoring the Cd, Se, and Ag binding energies across a range of Ag concentrations (0.38−1.83%, ICP−OES analysis) indicates no significant alterations to their chemical states as shown in the Supporting Information (Figure S2). Further, it is well-known that CdSe can undergo cation exchange with Ag to produce α-Ag$_2$Se.[39−41] However, if an exchange was occurring during the co-gelation the binding energies of both Ag
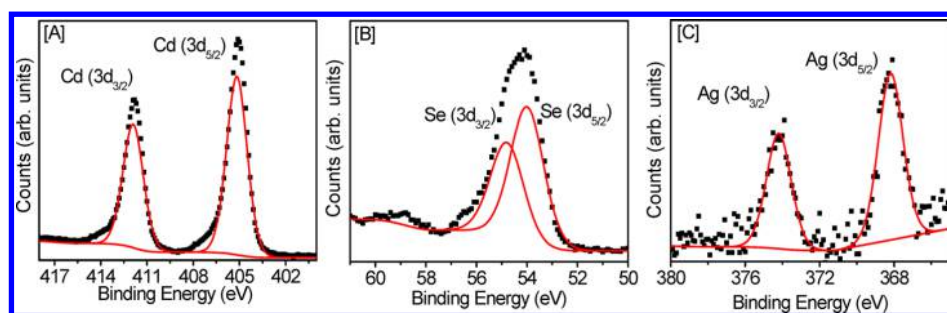
Figure 5. (A) Cd (3d$_{5/2}$), (B) Se (3d$_{5/2}$), and (C) Ag (3d$_{5/2}$) XPS spectra of CdSe/Ag aerogel with 1.83% Ag incorporation (ICP−OES analysis). The dotted lines are spectral data and the red lines are fitted deconvolutions.

TABLE 1. Comparison of Elemental Compositions, Absorption Band Onsets, Surface Areas, Average Pore Diameters, and Cumulative Pore Volumes of the CdSe/Ag Hybrid Aerogels

sample	elemental composition (ICP−OES)[a]		band gap[b] (eV)	surface area analysis		
	CdSe	Ag		surface area[c] (m^2/g)	avg pore diameter[d] (nm)	cumul pore volume[d] (cm^3/g)
1	100	0	2.21	202	15.9	0.916
2	99.73	0.27	2.20	202	15.0	1.120
3	99.49	0.51	2.18	200	15.8	1.071
4	99.47	0.53	2.18	210	18.2	0.889
5	99.37	0.63	2.08	187	16.4	0.819
6	99.19	0.81	2.07	131	18.4	0.656
7	98.70	1.30	2.04	97	18.8	0.514
8	98.54	1.46	1.97	87	17.0	0.406
9	98.27	1.73	1.93	81	16.3	0.400
10	98.17	1.83	1.82	69	19.4	0.316

[a] Weight % of Cd, Se, and Ag was calculated on the basis of ICP−OES analysis averaging three individual measurements per each composition. [b] Bandgaps were calculated by extrapolating the first absorption onset to the intersection point of the baseline.[1] [c] The Brunauer−Emmett−Teller (BET) model was applied to the nitrogen adsorption/desorption isotherms to investigate the surface area of aerogels. [d] The Barrett−Joyner−Halenda (BJH) model, which probes the pores in the size range of 1.7−300 nm, was applied to the nitrogen adsorption/desorption isotherms to investigate the porosity of aerogels.

and Se should shift to lower energies, which was not observed in any of the samples examined (Figure 5 and Supporting Information, Figure S2).[40,41] The lack of binding energy shifts in the hybrids suggests a physical mixing of the two components and no chemical ion exchange, in agreement with the PXRD data (Figure 4A), providing further evidence that evolving optical properties are not caused by the formation of α-Ag$_2$Se domains. However, it is well-known that metal−semiconductor interfaces can produce interface compounds,[42] and with the low concentrations of Ag loading, XPS may not be able to detect the interfacial interactions between CdSe and Ag NPs. It is likely that silver-reduced selenide (Ag−Se$^{n−}$) linkages exist at the interface, and presumably, these interactions facilitate the electron transfer between metal and semiconductor components. Nonetheless, studies involving resonance Raman and NMR spectroscopy are currently underway to further elucidate the chemical nature of interparticle interactions in CdSe/Ag hybrids.

The elemental compositions of the precursor NPs and aerogels were investigated from scanning electron microscopy/energy dispersive spectroscopy (SEM/EDS) and ICP−OES analyses. The low Ag content in the hybrid aerogels resulted in a statistically inaccurate measure of Ag composition through semiquantitative EDS. Therefore, ICP−OES was employed to probe the Cd, Se, and Ag compositions of the hybrids. Three individually prepared samples were analyzed per each composition, and the average results are presented in Table 1. In general, an increase in Ag content in the hybrid aerogels was noted with increasing concentration of Ag NPs in the hybrid sol. Consistent with ICP−OES, three prominent peaks were observed in the SEM/EDS spectra of hybrids, which were assigned to Cd, Se, and S (Supporting Information, Figure S3). The peaks corresponding to Ag and Cd exhibit major overlap, making it difficult to estimate the composition of individual metals. Nonetheless, EDS spectra indicate a significant decrease in sulfur content (19.09% and 20.99% in thiolate stabilized CdSe and Ag NPs, respectively, to 2.81−3.82% in CdSe/Ag aerogels), consistent with the oxidative removal of surface thiolates and direct cross-linking of metal and semiconductor components (Scheme 1).

The morphology and inner spatial distribution of CdSe and Ag NPs in the hybrid aerogels were investigated using transmission electron microscopy (TEM).
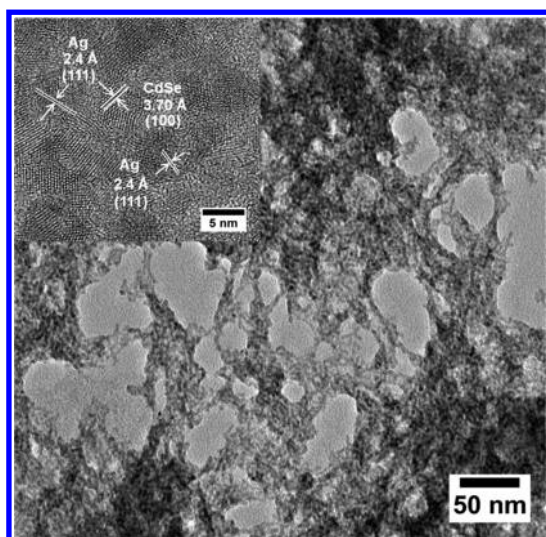
Figure 6. Representative low-resolution TEM image of the CdSe/Ag hybrid aerogels with 0.63% Ag composition. Inset shows the HRTEM image of a selected area. The dark contrast areas represent the multilayers of NPs showing the three-dimensional (3D) connectivity of NPs. The elemental composition was investigated by ICP−OES analysis.
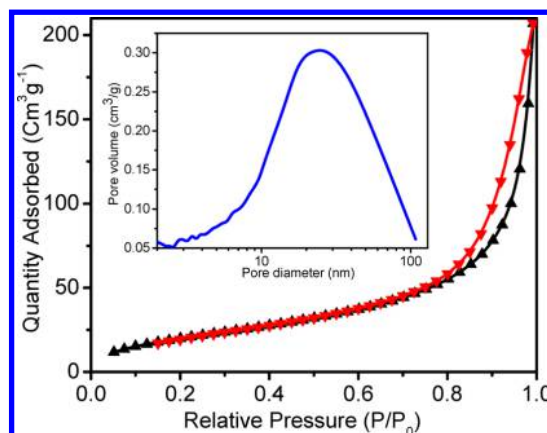

Figure 7. Representative nitrogen adsorption/desorption isotherm of CdSe/Ag aerogels with 0.81% Ag composition by ICP−OES. The inset shows the corresponding BJH modeled pore size distribution plot. The aerogel samples were degassed at 50 °C for 24 h prior to analysis.

The electron micrographs of the aerogels indicate the presence of nearly spherical colloidal NPs that are physically linked together to produce CdSe/Ag hybrids (Figure 6 and Supporting Information, Figure S4). The corresponding high-resolution TEM (HRTEM) images reveal the presence of CdSe and Ag NPs, as probed by the differences in (100) and (111) lattice spacings of hexagonal CdSe and cubic Ag, respectively (Figure 6 inset). Additional HRTEM images of the aerogels demonstrating the three-dimensionally (3D) connected network of CdSe and Ag NPs are shown in the Supporting Information (Figure S5). Further, SEM/EDS elemental maps indicating the random distribution of Ag NPs in the CdSe gel frameworks are shown in the Supporting Information (Figures S6−S8). These data are consistent with direct cross-linking of metal and semiconductor NPs, which allows direct electron tunneling and potentially novel optical properties. Moreover, the TEM analyses of hybrids indicate the highly porous morphology of aerogels, consisting of a range of mesopores (2−50 nm) and macropores (>50 nm) throughout the gel material. Consistent with the PXRD, the size estimations of NPs using TEM images revealed a slight decrease in particle size for CdSe and Ag NPs in the hybrids (Supporting Information, Figure S9) in comparison to precursor colloids (Figure 2A,B).

The surface areas of CdSe and CdSe/Ag hybrid aerogels were obtained by applying the Brunauer−Emmett−Teller (BET) model to nitrogen adsorption/desorption isotherms. A typical isotherm of the CdSe/Ag aerogel is shown in Figure 7 reflecting a combination of type IV and II curves, consistent with the formation of a meso-to-macroporous material.[28] The shape of the hysteresis loop is indicative of H1 and H3 character that corresponds to cylindrical- and slit-shaped pores, respectively.[32] The BET surface area of CdSe aerogels is 201−204 m^2/g, consistent with literature reports.[26] In contrast, CdSe/Ag hybrids exhibit surface areas in the range of 69−210 m^2/g depending on the Ag composition (Table 1). Recent reports on Ag aerogels indicate surface areas of 43−160 m^2/g,[28] while those of CdSe aerogels were 200−224 m^2/g.[32] Therefore, the incorporation of Ag NPs in the CdSe gel framework is likely to result in a decrease in the surface area with values that are intermediate of phase pure CdSe and Ag gel materials. In addition, as discussed previously the longer gelation time required with increased Ag loading leads to compaction and syneresis (solvent expulsion) of hydrogels resulting in dense monoliths that exhibit lower surface areas (d_{CdSe} = 0.032 g/cm^3 and $d_{CdSe/Ag}$ = 0.06−0.072 g/cm^3 for 1.3−1.83% Ag incorporation). This observation is further reflected in the cumulative pore volumes of the CdSe/Ag hybrids that exhibit a systematic decrease with increasing Ag concentration (Table 1). However, consistent with TEM images, small variations in average pore diameters (15−19.4 nm) were observed, suggesting the predominantly mesoporous nature of CdSe/Ag aerogels (Figure 6).

UV−vis absorption and PL spectra of hybrid aerogels were recorded to explore the influence of Ag on CdSe optical properties. Previous efforts on semiconductor−metal HNMs were mainly focused on enhancing the excitonic resonance through overlap with plasmonic energy levels to explore the optical trends.[15−17,20,21,43] In high interfacial contact systems such as core/shell heteronanostructures,[15,16] the formation of hybrid excitons was observed in the absence of PL, whereas in low interfacial contact systems systematic PL quenching was noted with no indication of the generation of hybrid states.[43] The implementation of sol−gel strategy allows for control over NP proximity as well
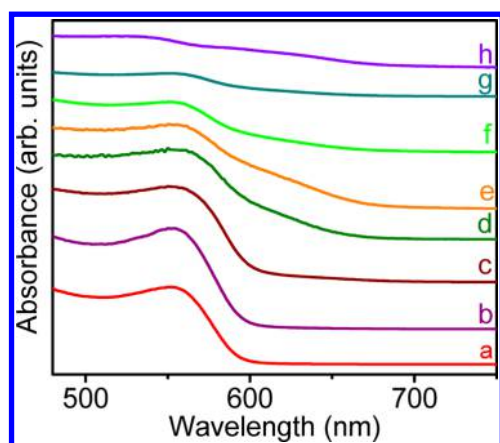
Figure 8. Solid-state absorption spectra of CdSe/Ag aerogels with (a) 0.00, (b) 0.53, (c) 0.81, (d) 1.07, (e) 1.30, (f) 1.83, (g) 2.01, and (h) 2.21% Ag composition. The elemental compositions of the aerogels were investigated by ICP−OES analysis.

as the concentration of metal and semiconductor components that can potentially minimize the FRET effects while maintaining the direct electronic contacts. Such controlled interfacial interactions are expected to blend the electronic energy levels of CdSe and Ag NPs without detrimental PL quenching effects. As a control study, the NPs surface passivated with thiolate ligands and mixed in solution exhibited no changes in optical properties regardless of Ag loading levels (Supporting Information, Figure S10). However, interesting optical trends were obtained upon oxidative removal of the surface ligands leading to the formation of low-dimensional CdSe/Ag hybrids.

The optical absorption of CdSe/Ag aerogels was investigated starting with very low Ag loading (0.13%), and the hybrids were systematically probed up to 2.21% Ag incorporation (Figure 8). All concentrations reported in the optical discussion are experimental values obtained from ICP−OES analysis. At very low levels of Ag loading (0.13−0.51%) no significant changes in the absorption band onsets were noted (Supporting Information, Figure S11), whereas at higher Ag content (0.53−2.21%) a systematic red shift, band tailing, and quenching effects of the absorption onsets were observed. The band tailing effect (Figure 8D−F) can be attributed to slightly inhomogeneous distribution of Ag NPs in the hybrids leading to regional differences in Ag concentration (Supporting Information, Figures S6−S8). When the Ag NPs are well dispersed in the hybrids (typically <0.81%) there is minimal alteration to the absorption properties (Figure 8A−C). Conversely, when the Ag NPs are more closely arranged in the aerogels (0.81−1.83%) overlapping electronic wave functions result in a progressive red shift of excitonic absorption and band-tailing effect. Further increasing the Ag composition (>2.01%) leads to significant depletion of CdSe absorption suggesting excessive loading of plasmonic NPs. The increased concentration of Ag could

possibly give rise to increased dipole−dipole interactions between metal and semiconductor NPs that result in band broadening and quenching of CdSe absorption.[22,23,29,44] In Figure 8G,H, although the absorption spectra appear to be completely quenched and the bandgap features are less distinguishable, the CdSe absorption is still present (Supporting Information, Figure S12). While strong quenching of absorption at 2.21% Ag loading is unexpected, similar band-tailing and quenching effects were reported for CdSe xerogels owing to a lower degree of confinement effects achieved in a dense NP network.[45] Likewise, the reduced porosity associated with the increasing Ag loading along with the effectively higher Ag concentrations achieved per unit area has the potential to rapidly quench the CdSe absorption. If the aerogels maintained the same porosity it is likely that the Ag induced changes would happen more slowly with increasing concentration.

The emission spectra of pure CdSe aerogels exhibit band-edge and trap-state emission maxima at 550 and 720 nm, respectively (Figure 9A).[26,32,46] With Ag loading as low as 0.13−0.53%, the band-edge emission quenches and a new emission at 630−640 nm emerges in between the band-edge and trap-state maxima of CdSe aerogels (Figure 9B). The temperature-dependent PL measurements of CdSe/Ag hybrids with 0.27−0.53% Ag loading demonstrate the dominant nature of the 640 nm emission peak (Figure 9B,C and Supporting Information, Figure S13). The presence of the band-edge and trap-state emissions in the hybrid aerogels with 0.27−0.53% Ag loading is further confirmed by additional time-resolved studies discussed below. The PLE spectra of the CdSe and CdSe/Ag hybrids probed at 550, 720, and 640 nm emission are consistent with the absorption studies and shown in the Supporting Information, Figure S14. The full width at half maxima of the fitted Gaussian peak of 640 nm emission (80 ± 20 nm, 0.31 ± 0.04 eV) is distinct from those of the band-edge (25 ± 10 nm, 0.11 ± 0.06 eV) and trap-state emission maxima (140 ± 30 nm, 0.42 ± 0.18 eV) of phase-pure CdSe aerogels supporting the view that the origin of new emission can be attributed to the emergence of an alternate radiative decay pathway.

To reveal the dynamics involving different relaxation pathways, TRPL spectroscopy was employed. All samples exhibit biexponential PL decays with slow and fast decaying components (Table 2), where the fast decays are most likely associated with surface and interfacial nonradiative recombination.[47] The CdSe aerogels exhibit PL decay times (τ_{slow}) of 1.83 ± 0.03 and 1190 ± 120 ns for the band-edge and trap-state emission bands (Figure 9D), respectively, which are consistent with the literature reports.[48−51] The corresponding decay times of CdSe/Ag hybrids with 0.27% Ag are 1.38 ± 0.05 and 944 ± 50 ns, respectively (Table 2). Interestingly, the main emission peak of the hybrid (640 nm) exhibits PL decay time of ∼600 ns, which is significantly longer
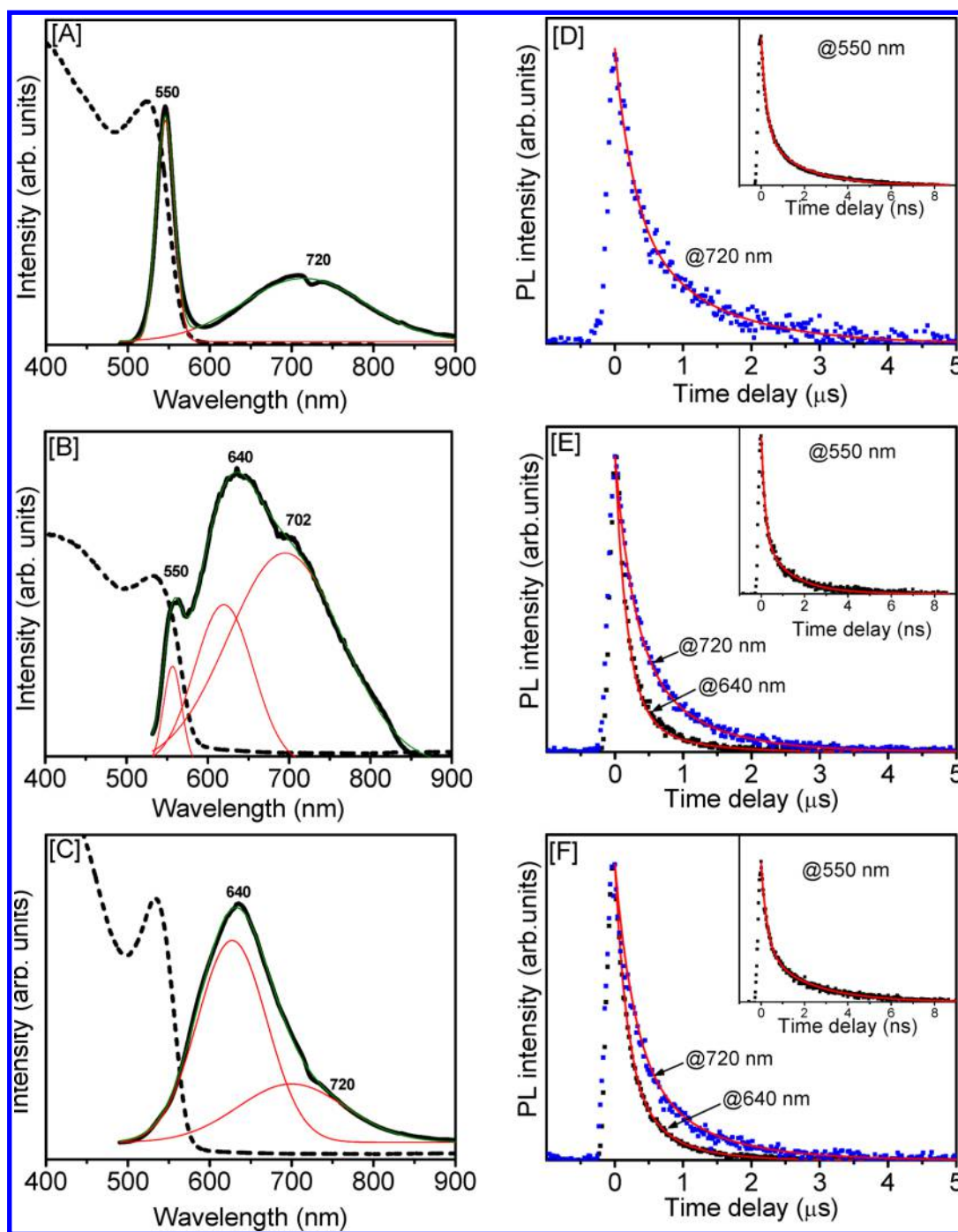
Figure 9. Solid-state absorption and PL spectra of CdSe/Ag hybrid aerogels with (A) 0.00, (B) 0.27, and (C) 0.53% Ag incorporation (ICP−OES analysis) along with the corresponding PL transients probed at band edge (550 nm) and trap state (720 nm) of CdSe aerogels and at the hybrid emission maxima (640 nm). In A−C, the black lines are spectral data, the red lines are fitted Gaussian peaks, and the green lines are the sum of all fitted peaks. The solid red lines in the TRPL decay spectra (D−F) represent the double-exponential fits. The absorption spectra were recorded at 300 K, whereas the PL and TRPL spectra were recorded at 15 K.

than that of the band-edge yet much shorter than that of the trap-state emission. To better understand the evolution of new emission, time-integrated PL spectra were recorded (Supporting Information, Figure S15). For CdSe/Ag hybrids (0.27% and 0.53% Ag), band-edge emission (550 nm) is predominant at the initial stages of the carrier recombination (integration time 50−100 ns)

because of its faster decay time. However, at longer time windows (integration time 200 ns−6.25 μs), band-edge emission is less predominant and the new emission at 640 nm dominates. It is important to note that at different Ag loading (0.27−0.53%), although the band-edge and trap-state emission peaks are very weak in steady-state PL spectra (Figure 9A−C), their presence

TABLE 2. Decay Times and Amplitude Ratios Obtained from Biexponential Fits, A_{fast} exp($-t/\tau_{fast}$) + A_{slow}exp($-t/\tau_{slow}$), to All Observed Emission Peaks of CdSe/Ag Aerogels with Different Ag Loading[a]

Ag composition (%)	τ_{slow} (ns)	τ_{fast} (ns)	A_{fast}/A_{slow}
	Band-Edge Emission of the CdSe/Ag Hybrids[b]		
0.00	1.83 ± 0.03	0.26 ± 0.01	1.94
0.27	1.38 ± 0.05	0.2 ± 0.01	1.95
0.53	2.18 ± 0.06	0.3 ± 0.01	1.75
	New Emission Peak of the CdSe/Ag Hybrids[b]		
0.27	685 ± 76	177 ± 6	5.15
0.53	596 ± 17	174 ± 3	2.35
	Trap-State Emission of the CdSe/Ag Hybrids[b]		
0.00	1190 ± 120	280 ± 28	1.37
0.27	944 ± 50	277 ± 12	1.75
0.53	986 ± 83	285 ± 19	1.76

[a] The elemental compositions were obtained from ICP—OES analysis. [b] Spectral windows used in the TRPL measurements are 500—560 nm for the band-edge emission, 600—660 nm for the hybrid emission, and 660—750 nm for trap-state emission. The average decay times obtained at different spectral windows are shown with standard deviations.

has been further confirmed by TRPL decay measurements (Figure 9E-F). Despite significant changes in absorption properties with increasing Ag composition beyond 0.53% (Figure 8), no change in emission properties were noted up to 1.83% Ag incorporation. All these observations support the view that the origin of new emission peak is a result of an alternate relaxation pathway introduced by incorporation of Ag NPs in the CdSe gel framework.

To explore a possible reasoning behind the formation of the hybrid emission two additional studies were conducted. Since FRET has been shown to depend on the energetic overlap of the donor/acceptor pairs, the CdSe/Ag hollow NP aerogels were produced to match the plasmonic absorption with the first excitonic energy.[17,43] The change in plasmon energy had no discernible effects on the hybrid emission, nor did the hollow NP shape affect the gel structure. Further discussion of this study is provided in the Supporting Information, Figure S16.

The lack of changes in the hybrid emission with varied plasmon energies prompted another study to explore the effects of changing the metal—semiconductor interfaces. Hybrid gels of CdSe/Au were studied at similar loading concentrations as in the case of CdSe/Ag gels. Although the plasmonic (535 nm) and excitonic energies (531 nm) were matched (Supporting Information, Figure S17) as in the CdSe/Ag hollow NP aerogels and similar gelation was noted, no trends in optical properties were observed through solid-state absorption and PL studies (Supporting Information, Figure S18). Unlike the CdSe/Ag aerogels, the absorption spectra of the CdSe/Au aerogels show no red shifting, but systematic quenching of the emission with increasing Au content.

Similar to previous studies on CdTe/Au aerogels,[22] strong PL quenching was noted even at low Au NP loadings (0.14—1.92%, Supporting Information, Figure S18).

The exact reason behind the different behaviors of Ag and Au in the gel structure has not yet been fully elucidated. However, a few possible explanations can be proposed on the basis of general semiconductor—metal interface theories. One potential reason is the difference in Fermi energy level (E_f) positions of Au vs Ag with respect to the conduction band (CB) and valence band (VB) of CdSe NPs.[22] The different Schottky barrier heights formed between CdSe/Ag and CdSe/Au would lead to differences in unique interface states within CdSe's bandgap. However, ideal Schottky barrier theory is a poor model to interpret actual interfaces due to chemical interactions. It is well-known that chemical reactivity also plays a role in metal—semiconductor interfaces and can result in lowering the Schottky barrier heights.[42] During the gelation process surface ligands are oxidized off and free active sites are created. When the metal and semiconductor NPs come in contact they will link together via Cd-metal or Se_n^{n-}—metal interfacial bonds. Similar Cd—Se_n^{n-} surface states and interparticle linkages are reported to exist in phase-pure CdSe aerogel superstructures.[36] From the comparison of heat of formation of AuSe (1.36 eV/metal atom) and Ag_2Se (0.52 eV/metal atom)[42] bonds, it can be anticipated that Ag will more readily bond to Se relative to Au. Furthermore, it has been shown that Au is one of the least reactive metals with respect to CdSe and while Ag is also considered unreactive it is more borderline to be reactive.[42] Previous studies on two-component gel materials have shown an increased reactivity of nanosized metal domains,[52] which could allow for Ag with borderline reactivity to more easily produce Ag—Se^{n-} interfacial bonds. As such, the preferred linkage of silver—chalcogenide bonds could possibly facilitate more favorable merging of energy levels and subsequent electron transfer across the interface and potentially account for the different optical properties observed in CdSe/Ag and CdSe/Au hybrids. Further, the surface Ag—Se^{n-} linkages are likely to cause a reduction in quantum confinement due to the addition of extra atomic layers. Therefore, the emission from Ag linked CdSe NPs could possibly arise from radiative relaxation of the exciton via a lower energy CB—VB transition. In addition, if Ag-linked CdSe NPs are acting as larger particles, several CB—VB energy transfers are possible, depending on the number of Ag NPs attached, causing the broad red emission. Moreover, it has been shown that dipole interactions between smaller and larger CdSe NPs can result in a long-range energy transfer and increased PL from the larger NPs.[53] Likewise, the direct interparticle linkages present in CdSe/Ag aerogels are likely to provide an alternative direct tunneling pathway for energy transfer. These interparticle energy transfers are

likely to account for the lower energy and the increased lifetime of the hybrid emission. Further studies, which are beyond the scope of this work, are underway to more completely understand the metal—semiconductor interfaces in CdSe/Ag hybrids and their effects on optoelectronic properties.

CONCLUSIONS

We have successfully produced CdSe/Ag aerogels composed solely of nanosized constituents via co-gelation of precursor particles. Oxidative removal of surfactant ligands gives rise to close interfacial contact that has potentially generated the novel optical properties. Physical characterization of the CdSe/Ag hybrids indicates the presence of an interconnected network of hexagonal CdSe and cubic Ag NPs. The nitrogen physisorption analyses revealed a decrease in the surface area and cumulative pore volume with increasing Ag loading owing to increased density of the hybrids. A systematic study on the evolution of optical properties of CdSe/Ag hybrids was performed via UV—visible, PL, and TRPL spectroscopies. Despite no significant changes in absorption onsets at low Ag content, a systematic red shift and band tailing effects were observed at high Ag content possibly due to excessive overlap of metal- semiconductor electronic wave functions. PL and TRPL analyses of CdSe/Ag hybrids (0.27% and 0.53% Ag) revealed the emergence of a new emission at ~640 nm with a decay time of ~600 ns, which is significantly different from those of the band-edge (1.83 ± 0.03 ns) and trap-state (1190 ± 120 ns) emission of CdSe aerogels, suggesting the generation of an alternate radiative decay pathway. The study of excitonic and plasmonic energy overlap has been extended with Ag hollow NPs and Au NPs, where PL quenching is the predominating effect with CdSe/Au hybrids. A potential explanation for this discrepancy has been proposed; suggesting more favorable interfacial chemical bonds between Ag with chalcogenides as opposed to Au. Gel morphology provides the opportunity to bring the NP surfaces in close contact, resulting in intermixing of their electronic states. Herein we introduced the co-gelation phenomena that optimizes the interfacial interactions of NP constituents to a moderate extent via the formation of fractal aggregates. This approach of coupling metal—semiconductor energies has the potential to impact a number of optical technologies including but not limited to biomedical, solar energy harvesting, and photocatalysis. Specific studies to test these premises are currently underway.

METHODS

Materials. Cadmium oxide (CdO, 99%), silver nitrate (AgNO$_3$, 99.9%), hydrogen tetrachloroaurate (III) hydrate (HAuCl$_4$, 49.0%), sodium borohydride (NaBH$_4$, 98%), n-tetradecylphosphonic acid (TDPA, 97%), trioctylphosphine (TOP, 97%), and tetramethylammonium hydroxide petahydrate (TMAOH, 97%) were purchased from Strem Chemicals. Trioctylphosphine oxide (TOPO, 99%), mercaptoundecanoic acid (MUA, 95%), L-glutathione reduced (98%), and tetranitromethane (TNM) were purchased from Sigma-Aldrich. Elemental Se (99+%), ethyl acetate, methanol (99+%), NaOH, and acetone (ACS grade) were purchased from Fisher Scientific. The water used in all syntheses was 18MΩ Mili-Q filtered, and all other chemicals were used as received.

Synthesis of CdSe Nanocrystals. CdSe NPs were produced by following a previously reported procedure[32] with slight modification to scale up the synthesis. In a typical reaction, 0.0514 g of CdO, 0.1116 g of TDPA, and 3.7688 g of TOPO were degassed under vacuum for 20 min at 100 °C and heated at 320 °C for 16 h under nitrogen flow to produce a homogeneous colorless solution. In a separate flask, 0.0316 g of Se was dissolved in 2.4 mL of TOP inside a nitrogen glovebox to produce a Se—TOP solution. The temperature of the Cd—TDPA—TOPO mixture was reduced to 270 °C, and the Se—TOP precursor was swiftly injected. The resultant mixture was allowed to cool to 150 °C, and the reaction temperature was slowly raised to 250 °C (10 °C/15 min). The resultant NPs were grown at 250 °C for 4 h and isolated and purified by multistep dispersion and precipitation using toluene and methanol, respectively.

Surface Functionalization of CdSe with Thiolate (MUA) Ligands. To facilitate more favorable gelation kinetics, the TOPO-capped CdSe NPs were subjected to a ligand exchange. The NPs were dispersed in 15 mL of 1.2 mM MUA in methanol after the pH was adjusted to ~10 with TMAOH. The solution was stirred under nitrogen for 2 h followed by the addition of an excess of ethyl acetate to precipitate the MUA-capped CdSe NPs. The resulting NPs were dispersed in 10 mL of mili-Q filtered water to produce 0.04 M CdSe sol.

Synthesis of GSH functionalized Ag NPs and Hollow Particles. The solid Ag NPs and hollow NPs were produced by employing a literature method.[33] In a typical synthesis, 4 mL of 10 mM AgNO$_3$ and 300 μL of 10 mM GSH were added to 50 mL of ice-cold Mili-Q water. Upon adjusting the pH to ~12 with 0.1 M NaOH, the solution color changed from colorless to pale yellow indicating the formation of Ag$_2$O NPs. Finally, 4.8 mL of 10 mM NaBH$_4$ was slowly added at a rate of 0.5 mL/min to produce dark brown solution of Ag NPs. In contrast, the rapid injection of NaBH$_4$ resulted in an immediate color change from pale yellow to orange brown suggesting the formation of hollow NPs. As-prepared Ag NPs and hollows were purified and concentrated using centrifuge filtration to produce 0.004 M Ag sols. The centrifuge filters (Sartorius, Vivaspin, 20 mL, MWCO 30000) filled with 20 mL of Ag sol were centrifuged at 3500g for 7—8 min to reduce the volume to 2—3 mL. The concentrated Ag sols were then mixed with 5—10 mL of mili-Q water and centrifuged to remove the residual byproducts (Na, NO$_3$, OH$^-$, and unreacted thiolates). Centrifuge filtration was performed multiple times to reduce the volume of the Ag sol to 10.0 mL (i.e., 0.004 M Ag) while retaining the colloidal stability of NPs.

Synthesis of GSH-Functionalized Au NPs. GSH-capped Au NPs were synthesized by following a literature method[54] with modification to scale up the synthesis. Briefly, 1.6 mL of 0.025 M HAuCl$_4$ and 700 μL of 0.019 M glutathione were added to 50 mL of ice-cold water, and the pH of the mixture was adjusted to 12 using 10 mL of 0.1 M NaOH. A freshly prepared 0.05 M NaBH$_4$ solution (2.0 mL) was swiftly injected that caused a color change from colorless to ruby-red, indicating the formation of GSH-capped Au NPs. The concentrated Au sols were produced using the centrifuge filtration as discussed above.

Synthesis of CdSe/Ag Hybrid Hydrogels and Aerogels. As-prepared CdSe sol (0.04 M) was divided into 1 mL aliquots, and varying volumes (0.1—0.9 mL) of Ag sol were added (Supporting Information, Table S1). The resultant mixtures were shaken vigorously to produce homogeneous solutions. With increasing Ag, the CdSe/Ag sols exhibit a progression of color from orange-red to deep brown-red. The gelation is induced by the addition

of 50 μL of 1% $C(NO_2)_4$ to hybrid sols, which yielded CdSe/Ag hydrogels after 2–6 h under ambient conditions.

The resulting hydrogels were aged for 1–2 days, and the byproducts of the oxidation were removed by exchanging with acetone 4–6 times over 2–3 days. The CdSe/Ag aerogels were produced by CO_2 supercritical drying (SCD). Porous microcapsules (SPI Supplies, Inc.) filled with acetone-exchanged wet gels were loaded into the SCD dryer and filled with liquid CO_2 at 15 °C. The acetone-treated gels were then exchanged with liquid CO_2 five to six times over 1–2 days. Finally, the wet gels were supercritically dried at 40 °C for 32 min to produce monolithic CdSe/Ag aerogels. CdSe/Au hydrogels and aerogels were produced using a similar procedure.

Characterization. The solution UV–vis absorption spectra of NPs were recorded using a Cary 6000i UV–vis–NIR spectrophotometer (Agilent Technologies). The reflectance spectra of aerogels were acquired using a diffuse reflectance (DRA) accessory attached to the UV–vis–NIR spectrophotometer and converted to absorption using the Kubelka–Munk remission function.[55] The solution PL measurements of CdSe NPs were performed using a Cary Eclipse fluorescence spectrophotometer (Agilent Technologies). Steady-state PL and TRPL studies were performed using a frequency doubled Ti:sapphire laser (385 nm wavelength, 150 fs pulse width, 160 kHz to 80 MHz repetition rate) as excitation source. On the detection end, a liquid N_2 cooled charge coupled device (CCD) camera connected to a spectrometer was employed to collect the steady-state PL spectra, and a Hamamatsu streak camera with 25 ps temporal resolution was used to analyze the PL transients. Powdered samples were deposited on glass substrates and mounted on a closed cycle He cryostat for TRPL analysis at 15 K. TEM were recorded in a JEOL JEM-1230 electron microscope equipped with a Gatan ultrascan 4000 camera operating at 120 kV. High-resolution TEM images were acquired in a field emission STEM-JEOL 2010F operating at 200 kV. Aerogels were suspended in ethanol via sonication (2–3 min) and dropped onto 200 mesh carbon-coated copper grids prior to analysis. A PAN analytical X'Pert PRO X-ray Diffractometer was used to record PXRD patterns of all samples. The average crystallite sizes were determined by applying the Scherrer equation[35] to (110) refection of CdSe and (111) reflection of Ag. XPS was performed using a Thermofisher ESCALAB 250 equipped with Al Kα source. Aerogel samples were pressed onto indium foil (Sigma-Aldrich) for analysis, and the surface-charging effect was corrected to advantageous carbon. The elemental compositions of the hybrid aerogels were investigated by ICP–OES and SEM/EDS techniques. The NP distribution in the aerogels were acquired through SEM/EDS elemental maps using a Hitachi FE-SEM SU-70 SEM operating at 20 keV. ICP–OES analyses were performed in a Varian VISTA-MPX instrument. The elemental composition of the Cd, Se, and Ag were obtained by monitoring five wavelengths per element. The aerogels were digested in 8 M HNO_3 acid, which was further diluted with ultrapure water prior to analysis. Densities of the aerogels were determined by employing a Micromeritics AccuPyc II 1340 gas pycnometer. Nitrogen physisorption isotherms were acquired at 77 K in a Micromeritics ASAP 2020 surface area and porosimetric analyzer. All samples were degassed under vacuum at 50 °C for 24 h before the analysis. A BET model was used to determine the surface area of aerogels. The pore size distributions, average pore diameters, and cumulative pore volumes were obtained by applying the BJH model to respective isotherms.

Conflict of Interest: The authors declare no competing financial interest.

Supporting Information Available: The Supporting Information is available free of charge on the ACS Publications website at DOI: 10.1021/acsnano.5b02777.

Photographs of monolithic hydrogels and aerogels of CdSe with different Ag concentration; Cd (3d), Se (3d), and Ag (3d)

XPS spectra of CdSe/Ag aerogels; SEM/EDS spectra of CdSe NPs, Ag NPs, and CdSe/Ag aerogels; solution UV–vis absorption spectra of CdSe/Ag hybrid sols; additional HRTEM images of CdSe/Ag NP and hollow particle based aerogels, optical characteristics of CdSe/Ag hollows and CdSe/Au hybrid aerogels; SEM/EDX mapping of Cd, Se, and Ag; histograms showing particles size in CdSe and CdSe/Ag hollow aerogels and molar concentration of CdSe and Ag NPs used in the hybrid gel formation (PDF)

REFERENCES AND NOTES

1. Esteves, R. J.; Ho, M. Q.; Arachchige, I. U. Nanocrystalline Group IV Alloy Semiconductors: Synthesis and Characterization of $Ge_{1-x}Sn_x$ Quantum Dots for Tunable Bandgaps. *Chem. Mater.* **2015**, *27*, 1559–1568.
2. Yu, J.; Xiang, Q.; Zhou, M. Preparation, Characterization and Visible-Light-Driven Photocatalytic Activity of Fe-Doped Titania Nanorods and First-Principles Study for Electronic Structures. *Appl. Catal., B* **2009**, *90*, 595–602.
3. Xiang, Q.; Yu, J.; Wang, W.; Jaroniec, M. Nitrogen Self-Doped Nanosized TiO_2 Sheets with Exposed {001} Facets for Enhanced Visible-Light Photocatalytic Activity. *Chem. Commun.* **2011**, *47*, 6906–6908.
4. Park, J. H.; Kim, S.; Bard, A. J. Novel Carbon-Doped TiO_2 Nanotube Arrays with High Aspect Ratios for Efficient Solar Water Splitting. *Nano Lett.* **2006**, *6*, 24–28.
5. Xiang, Q. J.; Yu, J. G.; Jaroniec, M. Nitrogen and Sulfur Co-Doped TiO_2 Nanosheets with Exposed {001} Facets: Synthesis, Characterization and Visible-Light Photocatalytic Activity. *Phys. Chem. Chem. Phys.* **2011**, *13*, 4853–4861.
6. Rajeshwar, K.; de Tacconi, N. R. Solution Combustion Synthesis of Oxide Semiconductors for Solar Energy Conversion and Environmental Remediation. *Chem. Soc. Rev.* **2009**, *38*, 1984–1998.
7. Dai, G.; Yu, J.; Liu, G. Synthesis and Enhanced Visible-Light Photoelectrocatalytic Activity of P-N Junction $BiOI/TiO_2$ Nanotube Arrays. *J. Phys. Chem. C* **2011**, *115*, 7339–7346.
8. Hou, W.; Cronin, S. B. A Review of Surface Plasmon Resonance-Enhanced Photocatalysis. *Adv. Funct. Mater.* **2013**, *23*, 1612–1619.
9. Xiao, M.; Jiang, R.; Wang, F.; Fang, C.; Wang, J.; Yu, J. C. Plasmon-Enhanced Chemical Reactions. *J. Mater. Chem. A* **2013**, *1*, 5790–5805.
10. Wang, P.; Huang, B.; Dai, Y.; Whangbo, M. H. Plasmonic Photocatalysts: Harvesting Visible Light with Noble Metal Nanoparticles. *Phys. Chem. Chem. Phys.* **2012**, *14*, 9813–9825.
11. Zhou, X.; Liu, G.; Yu, J.; Fan, W. Surface Plasmon Resonance-Mediated Photocatalysis by Noble Metal-Based Composites Under Visible Light. *J. Mater. Chem.* **2012**, *22*, 21337–21354.
12. Linic, S.; Christopher, P.; Ingram, D. B. Plasmonic-Metal Nanostructures for Efficient Conversion of Solar to Chemical Energy. *Nat. Mater.* **2011**, *10*, 911–921.
13. Costi, R.; Saunders, A. E.; Banin, U. Colloidal Hybrid Nanostructures: A New Type of Functional Materials. *Angew. Chem., Int. Ed.* **2010**, *49*, 4878–4897.
14. Li, J.; Zhang, J. Z. Optical Properties and Applications of Hybrid Semiconductor Nanomaterials. *Coord. Chem. Rev.* **2009**, *253*, 3015–3041.
15. Jiang, R. B.; Li, B. X.; Fang, C. H.; Wang, J. F. Metal/Semiconductor Hybrid Nanostructures for Plasmon-Enhanced Applications. *Adv. Mater.* **2014**, *26*, 5274–5309.
16. Zhang, W.; Govorov, A. O.; Bryant, G. W. Semiconductor-Metal Nanoparticle Molecules: Hybrid Excitons and the Nonlinear Fano Effect. *Phys. Rev. Lett.* **2006**, *97*, 1–4.
17. Zhang, J. T.; Tang, Y.; Lee, K.; Ouyang, M. Tailoring Light-Matter-Spin Interactions in Colloidal Hetero-Nanostructures. *Nature* **2010**, *466*, 91–95.
18. Samanta, A.; Zhou, Y. D.; Zou, S. L.; Yan, H.; Liu, Y. Fluorescence Quenching of Quantum Dots by Gold Nanoparticles: A Potential Long Range Spectroscopic Ruler. *Nano Lett.* **2014**, *14*, 5052–5057.

19. Kumar, A.; Chaudhary, V. Optical and Photophysical Properties of Ag/CdS Nanocomposites - An Analysis of Relaxation Kinetics of the Charge Carriers. *J. Photochem. Photobiol., A* **2007**, *189*, 272–279.

20. Gill, S. K.; Hope-Weeks, L. J. Monolithic Aerogels of Silver Modified Cadmium Sulfide Colloids. *Chem. Commun.* **2009**, *29*, 4384–4386.

21. Gill, S. K.; Brown, P.; Hope-Weeks, L. J. Gold Modified Cadmium Sulfide Aerogels. *J. Sol-Gel Sci. Technol.* **2011**, *57*, 68–75.

22. Hendel, T.; Lesnyak, V.; Kuehn, L.; Herrmann, A.; Bigall, N. C.; Borchardt, L.; Kaskel, S.; Gaponik, N.; Eychmueller, A. Mixed Aerogels from Au and CdTe Nanoparticles. *Adv. Funct. Mater.* **2013**, *23*, 1903–1911.

23. Lesnyak, V.; Wolf, A.; Dubavik, A.; Borchardt, L.; Voitekhovich, S. V.; Gaponik, N.; Kaskel, S.; Eychmueller, A. 3D Assembly of Semiconductor and Metal Nanocrystals: Hybrid CdTe/Au Structures with Controlled Content. *J. Am. Chem. Soc.* **2011**, *133*, 13413–13420.

24. Zhang, X.; Marocico, C. A.; Lunz, M.; Gerard, V. A.; Gun'ko, Y. K.; Lesnyak, V.; Gaponik, N.; Susha, A. S.; Rogach, A. L.; Bradley, A. L. Wavelength, Concentration, and Distance Dependence of Nonradiative Energy Transfer to a Plane of Gold Nanoparticles. *ACS Nano* **2012**, *6*, 9283–9290.

25. Brock, S. L.; Arachchige, I. U.; Kalebaila, K. K. Metal Chalcogenide Gels, Xerogels and Aerogels. *Comments Inorg. Chem.* **2006**, *27*, 103–126.

26. Mohanan, J. L.; Arachchige, I. U.; Brock, S. L. Porous Semiconductor Chalcogenide Aerogels. *Science* **2005**, *307*, 397–400.

27. Jeong, S. H.; Lee, J. W.; Ge, D.; Sun, K.; Nakashima, T.; Yoo, S. I.; Agarwal, A.; Li, Y.; Kotov, N. A. Reversible Nanoparticle Gels With Colour Switching. *J. Mater. Chem.* **2011**, *21*, 11639–11643.

28. Gao, X.; Esteves, R. J.; Luong, T. T. H.; Jaini, R.; Arachchige, I. U. Oxidation-Induced Self-Assembly of Ag Nanoshells into Transparent and Opaque Ag Hydrogels and Aerogels. *J. Am. Chem. Soc.* **2014**, *136*, 7993–8002.

29. Yu, H. T.; Liu, Y.; Brock, S. L. Tuning the Optical Band Gap of Quantum Dot Assemblies by Varying Network Density. *ACS Nano* **2009**, *3*, 2000–2006.

30. Yu, H.; Brock, S. L. Effects of Nanoparticle Shape on the Morphology and Properties of Porous CdSe Assemblies (Aerogels). *ACS Nano* **2008**, *2*, 1563–1570.

31. Yu, H.; Bellair, R.; Kannan, R. M.; Brock, S. L. Engineering Strength, Porosity, and Emission Intensity of Nanostructured CdSe Networks by Altering the Building-Block Shape. *J. Am. Chem. Soc.* **2008**, *130*, 5054–5055.

32. Arachchige, I. U.; Brock, S. L. Sol-Gel Assembly of CdSe Nanoparticles to Form Porous Aerogel Networks. *J. Am. Chem. Soc.* **2006**, *128*, 7964–7971.

33. Ben Moshe, A.; Markovich, G. Synthesis of Single Crystal Hollow Silver Nanoparticles in a Fast Reaction-Diffusion Process. *Chem. Mater.* **2011**, *23*, 1239–1245.

34. Detty, M. R.; Friedman, A. E.; Oseroff, A. R. A Mechanism for the Oxidation of Glutathione to Glutathione Disulfide with Organotellurium (IV) and Organoselenium (TV) Compounds - A Stepwise Process with Implications for Photodynamic Therapy and Other Oxidative Chemotherapy. *J. Org. Chem.* **1994**, *59*, 8245–8250.

35. Borchert, H.; Shevehenko, E. V.; Robert, A.; Mekis, I.; Kornowski, A.; Grubel, G.; Weller, H. Determination of Nanocrystal Sizes: A Comparison of TEM, SAXS, and XRD Studies of Highly Monodisperse CoPt$_3$ Particles. *Langmuir* **2005**, *21*, 1931–1936.

36. Pala, I. R.; Arachchige, I. U.; Georgiev, D. G.; Brock, S. L. Reversible Gelation of II-VI Nanocrystals: The Nature of Interparticle Bonding and the Origin of Nanocrystal Photochemical Instability. *Angew. Chem., Int. Ed.* **2010**, *49*, 3661–3665.

37. Katari, J. E. B.; Colvin, V. L.; Alivisatos, A. P. X-Ray Photoelectron-Spectroscopy of CdSe Nanocrystals with Applications to Studies of the Nanocrystals Surface. *J. Phys. Chem.* **1994**, *98*, 4109–4117.

38. Vargas-Hernandez, C.; Lara, V. C.; Vallejo, J. E.; Jurado, J. F.; Giraldo, O. XPS, SEM and XRD Investigations of CdSe Films Prepared by Chemical Bath Deposition. *Phys. Status Solidi B* **2005**, *242*, 1897–1901.

39. Chen, R. Z.; Xu, D. S.; Guo, G. L.; Tang, Y. Q. Electrodeposition of Silver Selenide Thin Films From Aqueous Solutions. *J. Mater. Chem.* **2002**, *12*, 1437–1441.

40. Jia, J.; Bendounan, A.; Kotresh, H. M.; Chaouchi, K.; Sirotti, F.; Sampath, S.; Esaulov, V. A. Selenium Adsorption on Au(111) and Ag(111) Surfaces: Adsorbed Selenium and Selenide Films. *J. Phys. Chem. C* **2013**, *117*, 9835–9842.

41. Yao, Q.; Arachchige, I. U.; Brock, S. L. Expanding the Repertoire of Chalcogenide Nanocrystal Networks: Ag$_2$Se Gels and Aerogels by Cation Exchange Reactions. *J. Am. Chem. Soc.* **2009**, *131*, 2800–2801.

42. Brillson, L. J. Transition in Schottky-Barrier Formation with Chemical Reactivity. *Phys. Rev. Lett.* **1978**, *40*, 260–263.

43. Okasha, A.; Mohamed, M. B.; Negm, S.; Talaat, H. Weak Exciton-Plasmon and Exciton-Phonon Coupling in Chemically Synthesized Ag/CdSe Metal/Semiconductor Hybrid Nanocomposite. *Phys. E* **2012**, *44*, 2094–2098.

44. Pankove, I. J. *Optical Processes in Semiconductors*; Dover Publications, Inc.: New York, 1971; pp 8−10.

45. Arachchige, I. U.; Mohanan, J. L.; Brock, S. L. Sol-Gel Processing of Semiconducting Metal Chalcogenide Xerogels: Influence of Dimensionality on Quantum Confinement Effects in a Nanoparticle Network. *Chem. Mater.* **2005**, *17*, 6644–6650.

46. Arachchige, I. U.; Brock, S. L. Sol-Gel Methods for the Assembly of Metal Chalcogenide Quantum Dots. *Acc. Chem. Res.* **2007**, *40*, 801–809.

47. Nirmal, M.; Murray, C. B.; Bawendi, M. G. Fluorescence-Line Narrowing in CdSe Quantum Dots-Surface Localization of the Photogenerated Exciton. *Phys. Rev. B: Condens. Matter Mater. Phys.* **1994**, *50*, 2293–2300.

48. Bawendi, M. G.; Carroll, P. J.; Wilson, W. L.; Brus, L. E. Luminescence Properties of CdSe Quantum Crystallites-Resonance Between Interior and Surface Localized States. *J. Chem. Phys.* **1992**, *96*, 946–954.

49. de Mello Donegá, C.; Bode, M.; Meijerink, A. Size and Temperature-Dependence of Exciton Lifetimes in CdSe Quantum Dots. *Phys. Rev. B: Condens. Matter Mater. Phys.* **2006**, *74*, 1–20.

50. Abdellah, M.; Karki, K. J.; Lenngren, N.; Zheng, K. B.; Pascher, T.; Yartsev, A.; Pullerits, T. Ultra Long-Lived Radiative Trap States in CdSe Quantum Dots. *J. Phys. Chem. C* **2014**, *118*, 21682–21686.

51. Jones, M.; Lo, S. S.; Scholes, G. D. Quantitative Modeling of the Role of Surface Traps in CdSe/CdS/ZnS Nanocrystal Photoluminescence Decay Dynamics. *Proc. Natl. Acad. Sci. U. S. A.* **2009**, *106*, 3011–3016.

52. Leventis, N.; Chandrasekaran, N.; Sadekar, A. G.; Mulik, S.; Sotiriou-Leventis, C. The Effect of Compactness on the Carbothermal Conversion of Interpenetrating Metal Oxide/Resorcinol-Formaldehyde Nanoparticle Networks to Porous Metals and Carbides. *J. Mater. Chem.* **2010**, *20*, 7456–7471.

53. Kagan, C. R.; Murray, C. B.; Bawendi, M. G. Long-Range Resonance Transfer of Electronic Excitations in Close-Packed CdSe Quantum-Dot Solids. *Phys. Rev. B: Condens. Matter Mater. Phys.* **1996**, *54*, 8633.

54. Brinas, R. P.; Hu, M.; Qian, L.; Lymar, E. S.; Hainfeld, J. F. Gold Nanoparticle Size Controlled by Polymeric Au(I) Thiolate Precursor Size. *J. Am. Chem. Soc.* **2008**, *130*, 975–982.

55. Nowak, M.; Kauch, B.; Szperlich, P. Determination of Energy Band Gap of Nanocrystalline SbSI Using Diffuse Reflectance Spectroscopy. *Rev. Sci. Instrum.* **2009**, *80*, 046107.